Hitless Wavelength Switching of Semiconductor Optical Amplifier-Integrated Reflection-Type Transversal Filter Laser With Suppressed Frequency Error

Yuta Ueda , *Member, IEEE*, Yusuke Saito , Takahiko Shindo , *Member, IEEE*,
Shigeru Kanazawa , *Senior Member, IEEE*, Wataru Kobayashi , Hideaki Matsuzaki, *Senior Member, IEEE*,
and Mitsuteru Ishikawa, *Member, IEEE*

Abstract—A spurious wavelength ($\lambda_{\text{spurious}}$) from a tunable laser during tuning is an issue in optical systems based on dynamically controlled laser wavelengths. Output shuttering synchronized with tunable-laser tuning is promising way to suppress $\lambda_{\text{spurious}}$. A semiconductor optical amplifier (SOA) is an ideal shutter for laser outputs with $\lambda_{\text{spurious}}$ in terms of low-wavelength-independent extinction ratio. We developed an electro-optically tunable reflection-type transversal filter (RTF) laser monolithically integrated with an SOA. Thanks to the nanosecond scale tuning speed of the RTF laser, the required shuttering time of the integrated SOA is also a corresponding nanosecond scale, which leads to little temperature change in the laser cavity. As a result, the laser frequency drift after turning off/on the SOA is suppressed to within $+/-2.5$ GHz without any additional laser control algorithm to compensate for the thermal crosstalk from the SOA. Using the laser, we demonstrated a "hitless" wavelength-switching subsystem based on a coherent format. Namely, outputs from an SOA-RTF laser coded with 32-GBd dual-polarization quadrature phase-shift keying (128 Gbps) are dynamically switched with $\lambda_{\text{spurious}}$ eliminated by SOA shuttering. In addition to practical bit error rates (BERs) of wavelength channels from the SOA-RTF laser, we observe no interference with the BER of a wavelength channel from another monitor laser in the wavelength-switching subsystem.

Index Terms—Coherent communications, electro-optic effect, high-speed tuning, semiconductor optical amplifier, tunable laser, wavelength switching.

I. INTRODUCTION

DYNAMIC control of a laser's wavelength is key technology for various optical systems. In a data center interconnection, optical switching using arrayed waveguide grating routers (AWGRs) and light sources whose wavelengths are dynamically switched is being discussed as a replacement for conventional electrical switching with large power dissipation and latency [1], [2], [3]. Optical switching is also expected to be applied for disaggregated computing in which hardware resources, such as processers, memories, and accelerators, are connected to each other through a large-bandwidth optical link [4]. Tunable lasers (TLs) with a high-speed tuning response play an important role in such novel optical communications architectures. In addition to communications, a high-speed TL is an indispensable component for remote sensing systems such as TDLAS (tunable diode laser spectroscopy) [5], [6], [7], [8], [9], [10] and LiDAR (light detection and ranging) [11], [12]. The tuning speed of a TL determines the number of data acquisitions per unit time, which contributes to not only increasing the time resolution of the system but also improving the signal to noise ratio by averaging repeatedly acquired samples.

An issue with TLs for practical applications using dynamic wavelength control is a spurious wavelength ($\lambda_{\text{spurious}}$) during tuning. For example, in the above-described optical router with an AWGR and TLs with wavelength switching (λ-switching), $\lambda_{\text{spurious}}$ from a TL manifests to another wavelength channel (λch), as shown in Fig. 1, when the AWGR has a certain amount of crosstalk. In this case, all nodes connected to an AWGR must synchronistically interrupt data transmissions, which limits the data link capacity and/or increases latency. Note that once a data link is interrupted to avoid crosstalk with a given period, it takes additional settling time to re-establish the commutations link, such as in a clock data recovery scheme [13].

Turning an active gain section (ACT) off/on in a laser cavity is the simplest approach to eliminating $\lambda_{\text{spurious}}$ from a TL. However, when one needs to reduce the laser linewidth of a TL, low noise is prioritized over a high-speed response in the electrical design for an ACT. For example, employing a low-noise current-supply IC and/or a large capacitor beside an ACT electrode results in a slow electrical response of the ACT. So, a semiconductor optical amplifier (SOA) is an ideal optical shutter because the ACT of a laser cavity does not have to be
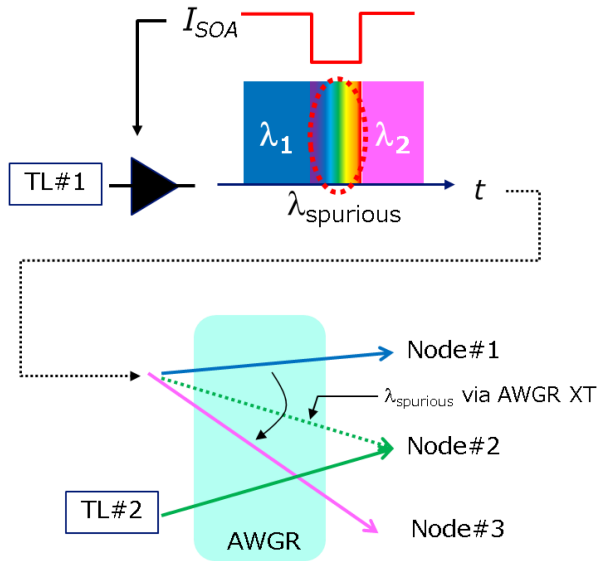
Fig. 1. Optical switching architecture based on λ-switching of TLs. In the illustrated example, the lasing wavelength from TL#1 is switched to λ_2 from λ_1 with $\lambda_{\mathrm{spurious}}$ during tuning, which interferences with the communications link of TL#2 via the AWGR crosstalk (XT). Eliminating $\lambda_{\mathrm{spurious}}$ of TL#1 by dynamically turning off/on an optical shutter such as an SOA is a practical approach for hitless communications of the TL#2 link.

Fig. 2. Photograph (top) and schematic (bottom) of SOA-RTF laser.

dynamically turned off/on. Furthermore, unlike an electro-absorption (EA) modulator [14], [15] and a Mach-Zehnder (MZ) modulator [16], [17], [18], it is possible to obtain a high extinction ratio (ER) without wavelength-dependent bias control proven in the form of SOA gate switches [19], [20]. A residual issue in using an SOA as an optical shutter is thermal crosstalk from the SOA to the laser cavity, which results in a laser frequency drift [21], [22], [23], [24], [25]. Methods of compensating for the drift include fast wavelength locking [22], using a dummy injection-current for thermal compensation [24], and optimizing tuning signals by an artificial-intelligence approach [25]. While these approaches are meaningful in terms of maximizing the performance of a given TL, implementation costs for additional electronics/optics components limit the application range of the TL.

In this paper, we describe an SOA-integrated electro-optically tunable reflection-type transversal filter (RTF) laser whose SOA functions as an optical shutter to eliminate $\lambda_{\mathrm{spurious}}$ during tuning. One feature of the electro-optically RTF laser is that the lasing wavelength is tuned by the electro-optic (EO) effect rather than the thermo-optic (TO) [26] or the free-carrier effect [27] employed in conventional TLs. Thanks to the nanosecond (ns)-scale response of the EO tuning of an RTF laser, the required SOA shuttering time is on a corresponding ns-scale, which is much shorter than the thermal response of the SOA, resulting in little temperature change of the laser chip. As a result, without employing dynamic frequency compensation, but with just supplying simple square-shaped current to the SOA, we confirmed frequency errors within $+/-2.5$ GHz even just after turning the SOA off/on. Another feature of the RTF laser is that the laser linewidth is on the order of hundreds of kilohertz regardless of the ns-scale tuning response, while laser linewidths of conventional TLs based on the free carrier effect with ns-scale
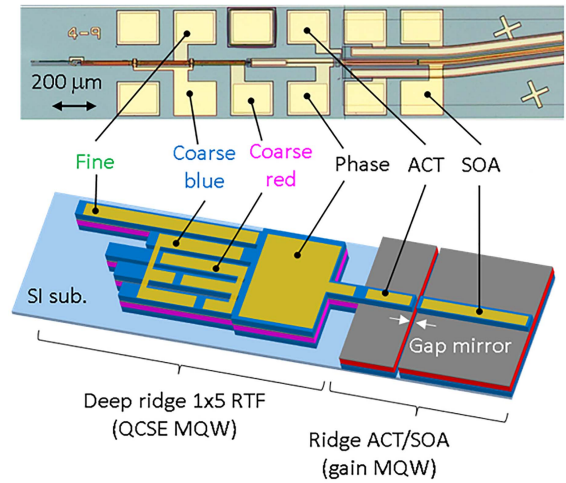
tuning time are typically over 1 MHz. We applied the SOA-RTF laser to a coherent-technology-based λ-switching system that imitates the subsystem shown in Fig. 1. Thanks to the successful elimination of $\lambda_{\mathrm{spurious}}$ using the SOA shutter, we achieved a hitless λ-switching in the subsystem [28]. That is, λchs of an SOA-RTF laser are successfully switched without degradation of the communication quality of the λch from another monitor laser [29].

II. DESIGN AND FUNDAMENTAL PERFORMANCE OF SOA-RTF LASER

A. Design and Fabrication

As described in the introduction, the laser wavelength of an RTF laser is tuned by the EO effect, whose tuning response is ns scale. This is much higher than the tuning speed of the TO effect (microsecond scale), which is a common tuning mechanism of recent narrow linewidth TLs. An electro-optically TL is also advantageous for narrow linewidth operation since free-carrier-induced noise is avoidable in a reverse-biased (carrier depletion) semiconductor p-i-n waveguide. Thus, it operates with a narrower linewidth than in carrier-injection-type TLs. In spite of the above high-speed response and narrow linewidth nature, the impractically small refractive index change (Δn) of the EO effect, which is $\sim 1/10$ of the TO and carrier effect, has been a barrier for an electro-optically TL with a practical tuning range. To overcome the barrier, we have compensated for the small Δn of the EO effect with a large filter tunability (a filter spectral shift for a given Δn) of the RTF as a wavelength selector, resulting in a full-C band operation of an RTF laser even with the EO tuning [30]. The laser exhibited about 350-kHz linewidth, the practically allowable linewidth for conventional digital coherent communications, and ns-scale λ-switching operation as expected.

Fig. 2 shows a photograph and schematic of an SOA-RTF laser that has an ACT, an SOA, and a tunable RTF region. Both the ACT and the SOA are made of the same InGaAsP-based multi-quantum well (MQW) with an optical gain in the 1.55-μm band.

The waveguides are ridge structures and are isolated with a 0.7-μm-gap mirror. Lengths of the ACT and SOA are 200 μm and 600 μm, respectively. The SOA is with a so-called angled facet with 7 deg. The tunable RTF section is made of an InAlGaAs-based MQW for the quantum-confined Stark effect (QCSE), which gives a Δn for the lightwave from the ACT. The RTF waveguide is a deep-ridge structure which consists of a 1 × 5 multi-mode interference coupler (MMI) and five reflection-type delay lines terminated with Au mirrors. We adopted 125 μm and 17 μm for the MMI length and width, respectively. The tuning mechanism of the RTF laser is as follows: (i) Broadband light from the ACT is divided into five beams through the 1 × 5 MMI. (ii) The five beams make a roundtrip in the delay lines with different optical lengths, resulting in the five beams' having different optical phases. (iii) The five beams are re-input into the 1 × 5 MMI and coupled at the ACT port with intensities depending on the phase relation among the five beams from the delay lines, which means the RTF functions as a wavelength filter.

Fig. 3(a) describes the dimensions of reflection-type delay lines whose lengths differ from the shortest line (reference delay line with a length L_0) by 0.5 × ($idL+\delta l_i$) ($i = 1, 2, 3$) and 0.5 × dL_{fine}. Note that because of the "reflection-type" delay line, the corresponding optical differential lengths are $idL+\delta l_i$ and dL_{fine}. Here, dL and dL_{fine} are differential lengths that determine the coarse and fine free spectral range (FSR) in an RTF spectrum shown in Fig. 3(b). Lengths of dL and dL_{fine} for an RTF described in this paper are chosen to be 15.6 μm and 312 μm. To compensate for the intrinsic phase property of the 1 × 5 MMI, minute lengths δl_i are added to delay lines. We set the lengths as ($\delta l_1, \delta l_2, \delta l_3$) = (−0.27, 0, 0.09) μm. More details on how to determine δl_i are described in our previous work [30], [32]. In Fig. 3(a), L_e represents a unit tuning-electrode length that determines a wavelength shift ($\Delta \lambda$) for a given Δn of a delay line as $\Delta \lambda \propto \Delta n L_e$. Red- and blue-shift tuning electrodes with lengths iL_e and $(3-i)L_e$ are installed on delay lines whose differential length is idL as also shown in Fig. 3(a). Note that the L_0 (reference delay-line length) has no influence on a reflectance spectrum of an RTF. Therefore, we can freely design the L_0 only if the laser-cavity length (longitudinal mode FSR) is practical. [33] Namely, we can adopt a long L_e under a geometrical condition $L_0 \geq 3L_e$ so that a practically large $\Delta \lambda$ is obtained even with a small Δn of the EO effect. Based on the seme policy as discussed in [33], L_0 and L_e are designed to be 600 μm and 180 μm.

A phasor diagram which represents a relative phase relation among beams from five delay lines are useful to understand a reflection spectrum of an RTF. Fig. 3(c) and (d) are phasor diagrams at relative wavelength points indicated in Fig. 3(b). Five phasors rotate as the relative wavelength changes. When we take a reflective index dispersion of a delay line into account, a relative phase change ($\Delta \phi$) of a beam from a delay line shown in Fig. 3(a) is proportional to an optical frequency change (Δf) rather than a wavelength change as follows ([30], [31], [32], also see Appendix 1):

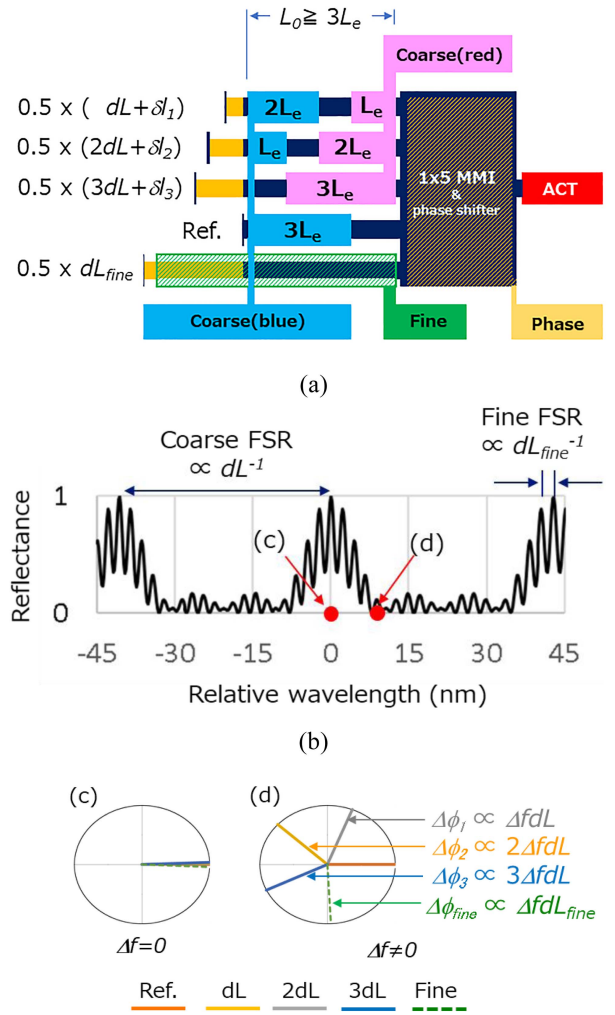$$\Delta \phi = 2\pi \Delta f \frac{n_g}{c} dL_x \qquad (1)$$

Fig. 3. (a) Delay-line dimensions of RTF laser. (b) Reflection spectra of RTF. (c) Phasor diagram at relative wavelength = 0 nm. (Δf =0) (d) Relative wavelength = 8 nm ($\Delta f \neq 0$). Five phasors [reference (ref.), dL, $2dL$, $3dL$, and fine] are distinguished by colors shown in legend.

Here, c and n_g are the speed of light in vacuum and a group index of a delay line, respectively. dL_x is a differential length ($dL_x = dL, 2dL, 3dL, dL_{fine}$). As shown in Fig. 3(c), when the relative wavelength is zero, namely $\Delta f = 0$, five phasors are in-phase, resulting in a maximum reflectance of an RTF. On the other hand, when the relative wavelength is finite ($\Delta f \neq 0$), five phasors are mismatched [Fig. 3(d)], which gives a small reflectance of an RTF. Note that we put the phasor of the beam from the "reference" delay line at a fixed position of $\Delta \phi = 0$ both in Fig. 3(c) and (d), since the RTF reflectance at a given relative wavelength point depends only on the relative phase relation among five phasors.

Fig. 4 shows the reflectance spectra of an RTF along with the phasor diagrams at relative wavelengths of 0 and +/−10 nm. In Fig. 4(a), optical phases of the five beams are in-phase at the relative wavelength of 0 nm, resulting in maximum reflectance of the RTF. By applying a voltage to the coarse-red tuning electrode, one can make all phasors other than the fine-delay line in-phase [Fig. 4(b)]. And, by biasing the fine-tuning electrode,
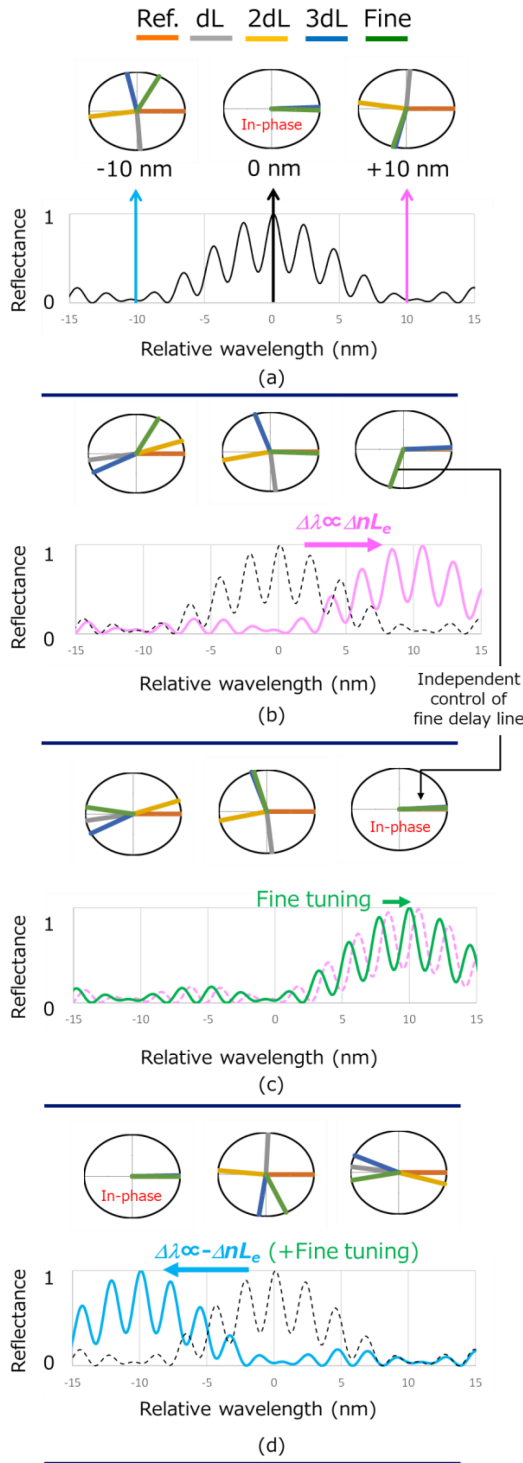
Fig. 4. Tuning mechanism of RTF laser. Reflection spectra and corresponding phasors at relative wavelength points of 0 and $+/-10$ nm. (a) Initial state. (b) Red coarse tuning. (c) Fine tuning for state (b). (d) Blue coarse tuning with fine tuning.
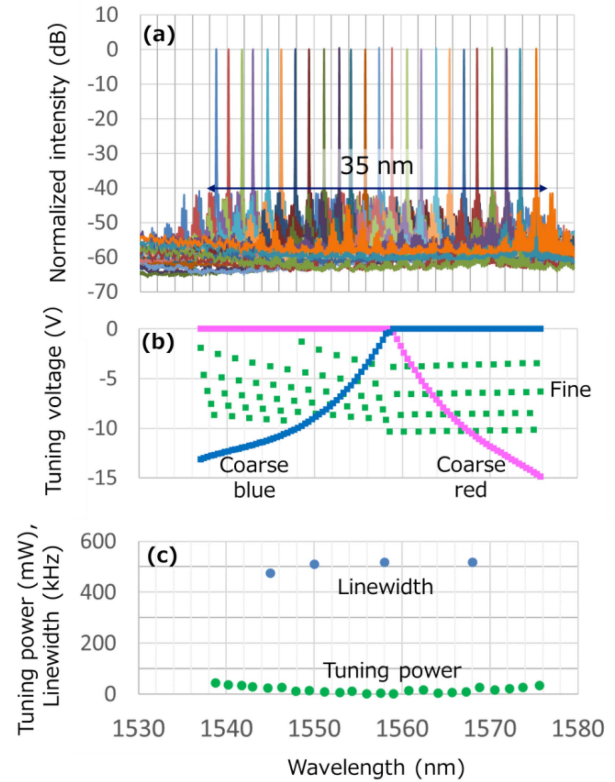

Fig. 5. Static tuning characteristics. (a) Lasing spectra. (b) Tuning voltages. (c) Tuning power dissipations and laser linewidths.

obtained by biasing the coarse-blue tuning electrode. Fig. 4(d) shows a reflectance spectrum whose maximum relative wavelength point is -10 nm. In the example shown in Fig. 4(d), fine tuning is also implemented with the coarse-blue tuning.

B. Fabrication and Fundamental Performance

The first epitaxial wafer (1st epi) in the fabrication process of an SOA-RTF laser contains the InAlGaAs-based MQW for the QCSE. Since an MQW with aluminum material is grown in a severe epitaxial growth condition such as an oxygen background [34], we choose the 1st epi with an InAlGaAs MQW. Namely, we partially replaced the MQW on the 1st epi with an InGaAsP-based MQW with an optical gain for the 1.55-μm band [35]. After the regrowth, we formed a deep ridge waveguide (RTF) and a ridge waveguide (ACT/SOA) on the InAlGaAs and InGaAsP MQW region, respectively, using a photolithographic process. The deep-ridge waveguide was formed by inductively coupled plasma reactive ion etching (ICP-RIE); the ridge waveguide was formed by methane/hydrogen based RIE and wet etching. The gap mirror between the ACT and SOA was formed in the same ICP-RIE batch used for forming the deep-ridge waveguide. Although the RTF waveguide is a high-contrast deep-ridge ($\sim$4-μm etching depth), we did not use any resin for planarization, such as benzocyclobutene, to avoid external stress to the waveguide, which would cause reflective index fluctuations [36].

Fig. 5(a) and (b) show lasing spectra of the SOA-RTF laser and corresponding coarse- and fine-tuning voltages applied to

the fine-delay-line phasor is independently controlled so that all phasors are in-phase [Fig. 4(c)]. Namely, while the envelop of the reflectance spectrum "coarsely" defines the lasing wavelength range, the short-interval ripples of the spectrum are for "finely" choosing one longitudinal mode. The blue-shift tuning is also

the laser. Phase tuning voltages [not displayed in Fig. 5(b)] were applied within 0 and −15 V so that each lasing wavelength fits the ITU grid [37]. All experimental data in this paper, including for Fig. 5, were obtained with an injected current into the ACT of 50 mA and a chip temperature of 45 °C. The absolute tuning voltages are less than 15 V for the 35-nm tuning of the laser. Tuning power dissipations and laser linewidths are plotted in Fig. 5(c). The tuning power, the sum of the products of applied voltages and corresponding photocurrents, is less than 50 mW. It should be noted that most of the 50 mW comes from photo-carrier extraction (carrier acceleration in the depletion layer) from the p-i-n structure of the RTF waveguide rather than from thermal energy. Therefore, applying tuning voltage to the RTF hardly influences the chip temperature, resulting in practically small thermal drift in λ-switching [33]. The thermal drift is difficult to be managed in conventional current-injection type TLs. The laser linewidths shown in Fig. 5(c) calculated from frequency-noise measurement results are ∼500 kHz. While we believe that the obtained linewidths are acceptable for conventional 100G coherent systems described in the next section, they are broader than those of our conventional RTF laser (∼350 kHz) without SOA integration. The broadening is most likely due to residual reflection from the SOA output facet. When a laser linewidth without external reflection ($\Delta\nu_0$) increases to $\Delta\nu$ by a weak reflection, a broadening factor ($\Delta\nu/\Delta\nu_0$) is theoretically expressed [38] as follows:

$$\frac{\Delta\nu}{\Delta\nu_0} \leq (1 - C)^{-2} \qquad (2)$$

Here, C (<1 for a weak external reflectance) represents a feedback parameter of an external reflection (see Appendix 2) and is proportional to an "effective" reflectance which is a product of the roundtrip SOA gain and the residual reflectance at the SOA facet. In the SOA-RTF laser, we estimate $C = 0.26$ with an SOA gain of 10 dB (20 dB for a roundtrip) and a reflectance of less than –40 dB for the angled SOA facet with an anti-reflection (AR) coating. This indicates that the conventional laser linewidth of an RTF laser without SOA (∼350 kHz) can increase by ∼85% in the worst case, which is roughly coincident with the obtained ∼500 kHz of the SOA-RTF laser. As also described in Appendix 2, we can obtain $C = 0.08$ (broadening factor ∼20%) by realizing the SOA reflectance with –50 dB. So, optimizing the AR coating condition is one approach to reducing the SOA-RTF laser linewidth.

Fig. 6 shows output powers from the SOA-RTF laser as a function of injection current. The measurement was performed for the SOA-RTF laser whose lasing wavelength is tuned to 1540, 1555, and 1575 nm. Although the outputs were obtained with an integrating sphere (no fiber-coupling loss), the output power exceeds +13 dBm, compliant with the practical specification [39], for the 35-nm wavelength band even with a 1-dB optical assembly margin in packaging. ERs of the SOA are over 40 dB regardless of the laser wavelength. Note that typical ERs of EA and MZ modulators are around 30 dB at most with wavelength-dependent bias control, which is not practical for the output shutter of a TL.
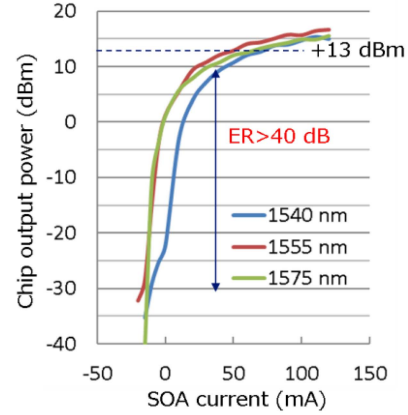

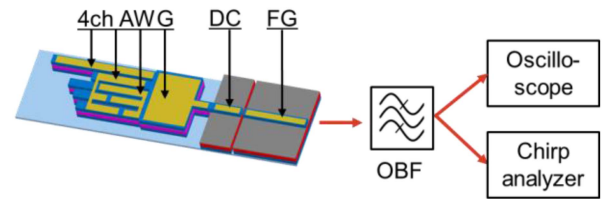Fig. 6. Output power as a function of SOA current.

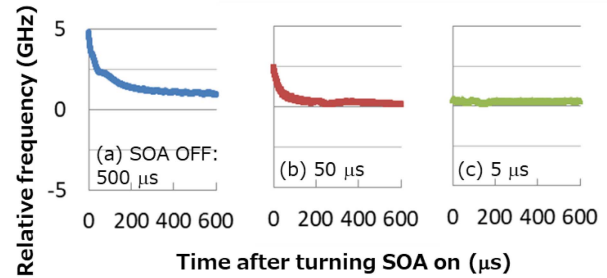Fig. 7. Measurement setup for dynamic laser frequency response.

Fig. 8. Laser-frequency drifts of SOA-RTF laser after turning SOA on. SOA-off time: (a) 500 μs, (b) 50 μs, and (c) 5 μs.

III. Dynamic Performance of SOA-RTF Laser

A. Transient Response of Laser Frequency

We investigated the dynamic laser wavelength/frequency characteristics of an SOA-RTF laser with the experimental setup shown in Fig. 7. A 4ch arbitrarily waveform generator (AWG) was used to supply sets of tuning voltages statically or dynamically to four tuning electrodes, namely, red-coarse, blue-coarse, fine, and phase. While a DC current was injected into the ACT, a modulation signal from a function generator (FG) was supplied to the SOA. The laser output was input into an optical band-path filter (OBF) with a full width at half maximum (FWHM) of 0.5 nm. After the light went through the OBF, it was input to an oscilloscope or an MZ-interferometer-type chirp analyzer with an FSR of 150 GHz.

First, we measured the relation between the laser-frequency drift and the SOA-shuttering time, as shown in Fig. 8. In the experiment, the SOA was turned off with −0.5 V after a 10-ms on-state with 1.5 V (∼70 mA) for settling laser frequency. In the
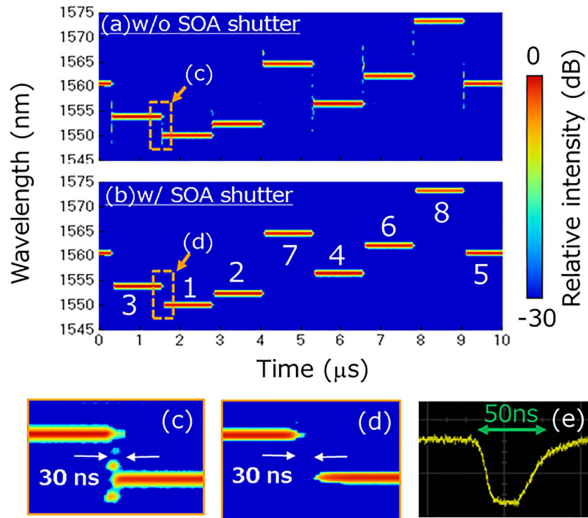
Fig. 9.   Time-wavelength maps of SOA-RTF laser (a) Without and (b) With SOA shuttering. (c) and (d) Corresponding enlarged views. (e) Laser intensity response in SOA shuttering.

Fig. 10.   Laser-frequency drifts in 8ch λ-switching with SOA shuttering.

experiment, the tuning voltages were fixed, namely the lasing wavelength was not intentionally controlled. Thus, the experiment was to extract the influence on the laser frequency drift purely due to the SOA-thermal effect. When the SOA-shuttering time was 500 μs [Fig. 8(a)], we observed decreases in the laser frequency (increases in the wavelength) for a 100-μs time scale after the turning the SOA on, which indicates that the laser cavity temperature drops during the SOA shuttering and rises again after re-starting the current injection into the SOA, leading to heat generation. However, when the SOA-shuttering time is as short as 50 μs [Fig. 8(b)], the laser-frequency fluctuation is around 2.5 GHz, which is a practically allowable frequency error [39]. Furthermore, the frequency error is ignorable if the shuttering is 5 μs [Fig. 8(c)]. The result means that if a λ-switching time of a TL is shorter than 5 μs, which is difficult for a conventional TO-tuning TL, the corresponding SOA-shuttering time no longer affects the laser frequency.

Next, we obtained time-wavelength maps (t-λ maps) of an SOA-RTF laser whose lasing wavelength was dynamically changed as cyclic 8ch λ-switching, as shown in Fig. 9(a) and (b). The experimental setup is shown in Fig. 7. The map was obtained by repeatedly shifting the center wavelength of the OBF and capturing a waveform displayed on the oscilloscope. While the SOA is statically biased with 1.5 V (∼70 mA) [Fig. 9(a)], it is dynamically turned off (−0.5 V) and on (1.5 V) at the timing of the λ-switching [Fig. 9(b)]. Fig. 9(c) and (d) are enlarged views corresponding to indicated points in Fig. 9(a) and (b), respectively.

In Fig. 9(a) and (c), one can clearly observe $\lambda_{\text{spurious}}$ of the laser in the 30-ns λ-switching time, which reflects the dynamically tuned reflectance spectrum of the RTF. The 30-ns is due to the slew rate of the 4ch AWG. In fact, the RTF laser has sub-ns λ-switching potential [30]. However, the λ-switching of 30 ns is fast enough to suppress the laser frequency error due to the thermal effect of the SOA, as discussed in Fig. 8 and further
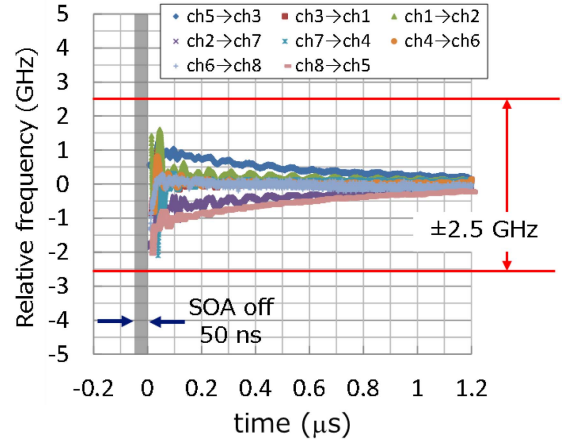
proven later in this section. In contrast to the t-λ map shown in Fig. 9(a), the $\lambda_{\text{spurious}}$ is successfully eliminated with an over 30-dB dynamic ER (measurement limit) by synchronously turning the SOA off/on. The intensity waveform at the timing of the SOA shuttering is shown in Fig. 9(e).

As described in Fig. 8, little frequency drift of the SOA-RTF laser is expected in the SOA-shuttering because the ns-scale shuttering time results in little change in the cavity temperature. We measured the temporal laser frequency of the SOA-RTF laser at all λ-switching timings in the experimental condition of Fig. 9(b). The experimental setup was the same as shown in Fig. 7. Fig. 10 shows the measured relative frequency drifts. For all λ-switching patterns, we confirmed suppressed frequency errors within $+/-2.5$-GHz as expected. It should be noted that, for example, in the case of λ-switching from ch8 to ch5, the laser frequency increases (wavelength decreases) after tuning the SOA on, which is not observed in Fig. 8. The increase in the laser frequency is caused by a slight change in the photocurrents, which is less than 1 mA per tuning electrode, resulting in a change in Joule heating in the tuning electrodes. This indicates that the frequency drift is no longer influenced by the thermal crosstalk from the SOA.

From the above discussions, we have clarified that the ns-scale λ-switching of the SOA-RTF laser is effective for minimizing the SOA-shuttering time to eliminate $\lambda_{\text{spurious}}$ in the λ-switching, resulting in little frequency error due to the SOA-thermal crosstalk. The practical advantage of this nature of the SOA-RTF laser is that no additional laser-frequency control algorithm, such as dynamic control of phase-tuning or dummy injection-current into a laser chip, is needed for wavelength drift compensation. In addition to optical communications use, the low frequency error with SOA shuttering is also suitable for remote sensing systems using a laser frequency such as coherent LiDAR [11], [40].

B. Hitless λ-Switching Using SOA Shuttering

As described in the introduction, λ-switching using a TL without $\lambda_{\text{spurious}}$ is advantageous in optical switching systems because interrupting other communications channels to avoid
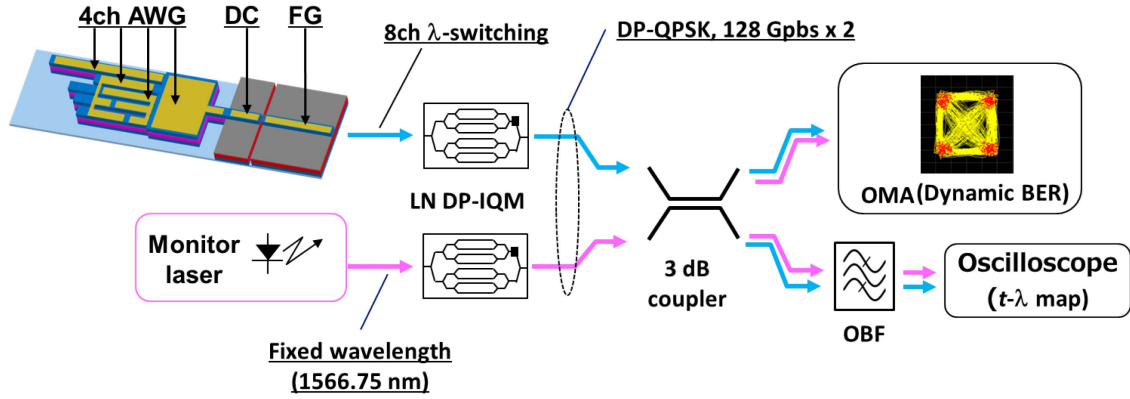
Fig. 11. Setup for demonstration of hitless λ-switching of SOA-RTF laser.

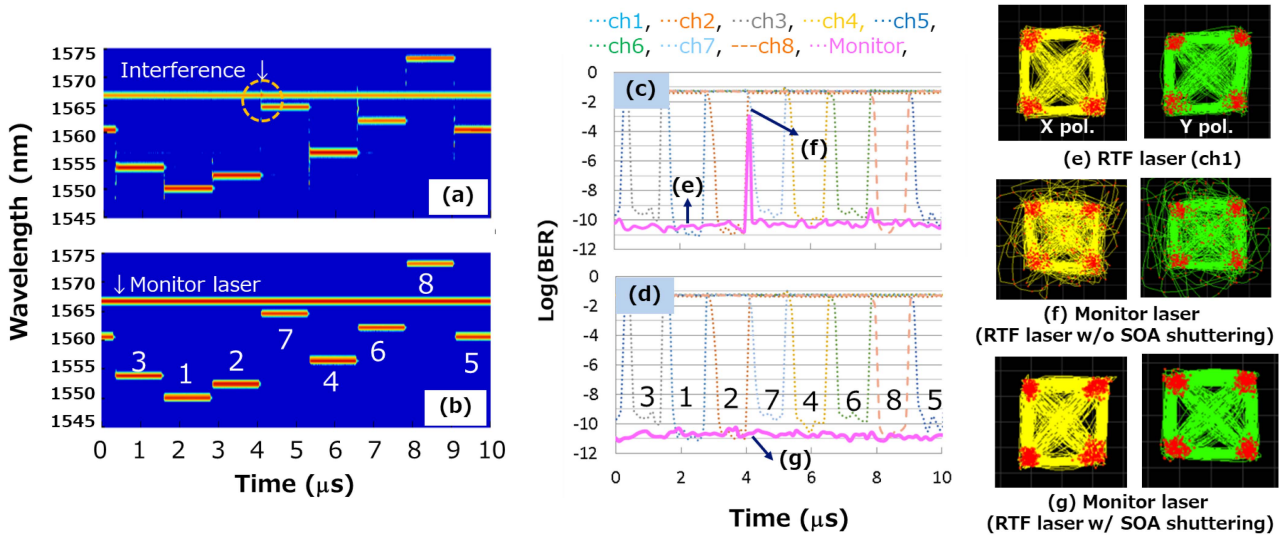Fig. 12. Hitless λ-switching demonstration results. (a) t-λ map of monitor laser and SOA-RTF laser without SOA shuttering. (b) With shuttering. (c) Dynamic BER without SOA shuttering. (d) With shuttering. (e) Constellation maps of SOA-RTF laser ch1 for X and Y polarization (pol.). (f) Monitor laser channel without SOA-shuttering. (g) With shuttering.

crosstalk light from the switched TL is unnecessary, that is, hitless optical switching is possible.

We demonstrated hitless λ-switching using the SOA-RTF laser with the experimental setup shown in Fig. 11. We prepared two lasers: an SOA-RTF laser and a commercially available laser as a monitor laser. While the SOA-RTF laser operates in the same cyclic 8ch λ-switching condition as in the experiment shown Fig. 9(a) and (b), the laser wavelength of the monitor laser is fixed at 1566.75 nm. Each laser output was input into commercially available lithium niobate (LN) modulator and modulated in the form of 32-GBd dual-polarization quadrature phase shift keying (DP-QPSK). The pair of DP-QPSK signals from the two lasers were coupled with a 3-dB coupler which imitates an optical router. Then, the mixed optical signals were input into an optical modulation analyzer (OMA). The mixed output was also input into the same t-λ map setup composed of an OBF and an oscilloscope.

Fig. 12(a) and (b) show t-λ maps obtained in the demonstration. When the SOA-RTF laser operates *without* SOA shuttering [Fig. 12(a)], $\lambda_{spurious}$ interferes with the monitor laser channel

at the λ-switching of the SOA-RTF laser from ch2 to ch7. On the other hand, the interference is avoided when the laser operates *with* SOA shuttering [Fig. 12(b)]. Note that the FWHM of the OBF for the t-λ map shown in Fig. 12(a) is 0.5 nm (∼64 GHz) and the optical signal is modulated at 32 GBd in the experiment. So, even when the optical frequency distance between $\lambda_{spurious}$ and monitor laser wavelength is over 32 GHz (little influence on the signal quality of the monitor laser channel), the two wavelengths seem to overlap [e.g., SOA-RTF laser from ch4 to ch6 in Fig. 12(a)]. In addition, during λ-switching, a multi-mode lasing is possible as understood from Fig. 9(c). In such a multimode lasing sate, one wavelength intensity of $\lambda_{spurious}$ is smaller than a monitor laser intensity. This means that even when $\lambda_{spurious}$ exists in the signal bandwidth of the monitor laser channel, the influence of $\lambda_{spurious}$ can be limited depending on the $\lambda_{spurious}$ intensity.

Fig. 12(c) and (d) display dynamic bit-error rates (BERs) of modulated light from the SOA-RTF laser and monitor laser. While eight dot lines represent dynamic BERs of eight λchs from the SOA-RTF laser, the bold pink line shows the dynamic

BER of the λch from the monitor laser channel. These dynamic BERs were calculated from corresponding constellation maps. Fig. 12(e) shows the constellation maps for X and Y polarization (pol.) of the ch 1 from the SOA-RTF laser. The optical signal-to-noise ratio (OSNR) of each λch is set to about 30 dB in the demonstration. Dynamic BERs of less than 10^{-9} were obtained from the SOA-RTF laser operating as 8ch λ-switching, which indicates the high-speed and narrow-linewidth nature of the laser.

As expected from the experimental results in Fig. 12(a), the dynamic BER of the monitor-laser channel degrades due to $\lambda_{spurious}$ from the SOA-RTF laser without SOA shuttering [Fig. 12(c)]. That is, the $\lambda_{spurious}$ from the SOA-RTF laser is coupled with the monitor-laser channel, resulting in disturbed constellation maps [Fig. 12(f)]. The BER degradation is improved when the SOA shuttering is applied to the SOA-RTF laser, as shown in Fig. 12(d), thanks to successfully eliminated $\lambda_{spurious}$ from the SOA-RTF laser. The BER improvement is also clear from the comparison between constellation maps shown in Fig. 12(f) and (g).

IV. CONCLUSION

In this paper, we described an RTF laser monolithically integrated with an SOA, which is used to eliminate $\lambda_{spurious}$ during tuning. Thanks to the 30-ns tuning time (driver limit) of the RTF laser, the required SOA shuttering time is also ns scale, which hardly influences cavity temperature, resulting in frequency error within $+/-2.5$ GHz even just after turning the SOA off/on. The only additional laser control scheme is a simple square-shaped current supplied to the SOA, which minimizes application costs of a TL to an optical system with dynamically controlled laser wavelengths. We also demonstrated a λ-switching subsystem with an SOA-RTF laser operating as 8ch λ-switching and a fixed-wavelength monitor laser. We confirmed hitless λ-switching in the subsystem; namely, the dynamic BER of the monitor-laser channel is not degraded even at the timing of λ-switching of the SOA-RTF laser with SOA-shuttering operation. The results prove that, in addition to speeding up optical systems, the ns-scale tuning response of the electro-optically tunable RTF laser is also advantageous for suppressing $\lambda_{spurious}$ with accurate laser frequency.

APPENDIX 1
DERIVATION OF (1)

When a beam propagates in a waveguide with a refractive index n and a length L, we define an optical phase ϕ, taking the wavelength dispersion of n account into, as follows:

$$\phi \;=\; -\frac{2\pi}{\lambda}nL \;=\; -\frac{2\pi}{\lambda}\left(\frac{dn}{d\lambda}\lambda + n_g\right)L \qquad \text{(A.1)}$$

Here, λ and n_g are the beam wavelength and the group refractive index of the waveguide, respectively. So, a phase difference ($\Delta\phi$) between beams with two different wavelengths ($\Delta\lambda$) are expressed as follows:

$$\Delta\phi \;=\; -2\pi n_g\left(\frac{1}{\lambda+\Delta\lambda} - \frac{1}{\lambda}\right)L \;=\; 2\pi\Delta f\frac{n_g}{c}L \quad \text{(A.2)}$$

In (A.2), c and Δf represent the speed of light in vacuum and an optical frequency difference corresponding to $\Delta\lambda$. Note that, in this paper, Δf is defined so that sings of $\Delta\lambda$ and Δf are the same. Namely, for $\Delta\lambda>0$ (increase in the optical wavelength), the corresponding optical frequency change is $-\Delta f (<0)$. When one needs to discuss a "relative" phase change between beams propagating in lengths L and L_0 (reference length), L in (A.2) is replaced with $L-L_0 (= dL_x)$, resulting in (1).

APPENDIX 2
DEFINITION OF C IN (2)

The feedback parameter C in (2) for a laser cavity with an external reflection is discussed in [38]. The definition is as follows.

$$C \equiv \frac{\left(1-r_c^2\right)r_m}{r_c}\frac{\tau_{ext}}{\tau_c}\sqrt{1+\alpha^2} \qquad \text{(A.3)}$$

Here, r_c and r_m are reflection coefficients at a main cavity output facet and an external facet. τ_c and τ_{ext} are roundtrip times of lightwave propagating in the main and the external cavity, respectively. And α is a linewidth enhancement factor, whose typical value is 3-5 for general MQWs. Note that the relation of (A.3) is valid when τ_{ext} is shorter than a coherence time of the laser. In the SOA-RTF laser described in this paper, r_c corresponds to the reflectance at the gap mirror which is designed to be $0.3^{0.5}$ ($r_c^2 = 0.3$) which is the same as a reflectance at a cleaved facet of our conventional RTF laser without SOA. When it comes to r_m, we need to consider the SOA roundtrip gain (10 dB $\times$ 2) in addition to the reflectance of the SOA facet (-40 dB) with an AR coating as described in the paper. So, the "effective" reflectance is 20 dB–40 dB $= -20$ dB, resulting in $r_m = 10^{-20/20} = 0.1$. If we assume the group velocities in the main and the external cavity are the same, τ_{ext}/τ_c in (A.3) becomes a ratio between two cavity lengths. As shown in Fig. 2, the main cavity length of the SOA-RTF laser is ~1200 μm. And as also described in the paper, the external cavity length (namely, SOA length) is 600 μm, resulting in $\tau_{ext}/\tau_c = 0.5$. Therefore, if we assume $\alpha = 4$, we obtain $C = \sim 0.26$. With the same scheme, $C = \sim 0.08$ for an SOA-facet reflectance of –50 dB.

REFERENCES

[1] K. Sato, "Realization and application of large-scale fast optical circuit switch for data center networking," *J. Lightw. Technol.*, vol. 36, no. 7, pp. 1411–1419, Apr. 2018.

[2] K. Suzuki, K. Yonenaga, N. Takachio, T. Tanaka, O. Moriwaki, and H. Onaka, "Device response time reduction for large-scale and fast optical switching systems," in *Proc. IEEE Opt. Fiber Commun. Conf.*, 2021, pp. 1–3.

[3] A. S. Raja et al., "Ultrafast optical circuit switching for data centers using integrated soliton microcombs," *Nature Commun.*, vol. 12, no. 1, pp. 1–7, 2021.

[4] M. Glick et al., "PINE: Photonic integrated networked energy efficient datacenters (ENLITENED program)," *J. Opt. Commun. Netw.*, vol. 12, no. 12, pp. 443–456, 2020.

[5] M. P. Arroyo and R. K. Hanson, "Absorption measurements of water-vapor concentration, temperature, and line-shape parameters using a tunable InGaAsP diode laser," *Appl. Opt.*, vol. 32, no. 30, pp. 6104–6116, 1993.

[6] M. G. Allen, "Diode laser absorption sensors for gas-dynamic and combustion flows," *Meas. Sci. Technol.*, vol. 9, pp. 545–562, 1998.

[7] O. Witzel et al., "VCSEL-based, high-speed, in situ TDLAS for in-cylinder water vapor measurements in IC engines," *Opt. Exp.*, vol. 21, no. 17, pp. 19951–19965, 2013.

[8] Y. Ueda et al., "2-μm band active distributed Bragg reflector laser for CO_2 gas sensing," *Appl. Phys. Exp.*, vol. 12, no. 9, 2019, Art. no. 092011.

[9] T. Shindo et al., "2.0-μm wavelength superstructure-grating-(SSG-) distributed Bragg reflector laser with tuning range of over 50 nm," *IEEE Photon. Technol. Lett.*, vol. 33, no. 13, pp. 641–644, Jul. 2021.

[10] T. Shindo et al., "51-nm uniform-intensity tuning of superstructure grating active-DBR laser for 2-μm wavelength band," *IEEE Photon. J.*, vol. 14, no. 3, Jun. 2022, Art. no. 1529708.

[11] C. V. Poulton et al., "Coherent solid-state LIDAR with silicon photonic optical phased arrays," *Opt. Lett.*, vol. 42, no. 20, pp. 4091–4094, 2017.

[12] H. Ito et al., "Wide beam steering by slow-light waveguide gratings and a prism lens," *Optica*, vol. 7, no. 1, pp. 47–52, 2020.

[13] K. A. Clark et al., "Synchronous subnanosecond clock and data recovery for optically switched data centres using clock phase caching," *Nature Electron.*, vol. 3, pp. 426–433, 2020.

[14] Y. Ueda, T. Fujisawa, S. Kanazawa, W. Kobayashi, K. Takahata, and H. Ishii, "Very-low-voltage operation of Mach-Zehnder interferometer-type electroabsorption modulator using asymmetric couplers," *Opt. Exp.*, vol. 22, no. 12, pp. 14610–14616, 2014.

[15] Y. Ueda et al., "Low driving voltage operation of MZI-type EA modulator integrated with DFB laser using optical absorption and interferometric extinction," *IEEE J. Sel. Topics Quantum Electron.*, vol. 21, no. 6, Nov./Dec. 2015, Art. no. 1501306.

[16] N. Kikuchi et al., "80-Gb/s low-driving-voltage InP DQPSK modulator with an n-p-i-n structure," *IEEE Photon. Technol. Lett.*, vol. 21, no. 12, pp. 787–789, Jun. 2009.

[17] Y. Ueda, Y. Ogiso, and N. Kikuchi, "InP PIC technologies for high-performance Mach-Zehnder modulator," *Proc. SPIE*, vol. 10129, 2017, Art. no. 1012905.

[18] J. Ozaki et al., "500-Gb/s/λ operation of ultra-low power and low-temperature-dependence InP-based high-bandwidth coherent driver modulator," *J. Lightw. Technol.*, vol. 38, no. 18, pp. 5086–5091, Sep. 2020.

[19] K. Morito, "Optical switching devices based on semiconductor optical amplifiers," in *Proc. IEEE Int. Conf. Photon. Switching*, 2009, pp. 1–2.

[20] G. Nakagawa et al., "Ultra-high extinction ratio and low cross talk characteristics of 4-array integrated SOA module with compact-packaging technologies," in *Proc. IEEE Eur. Conf. Exhib. Opt. Commun.*, 2011, pp. 1–3.

[21] L. Ponnampalam et al., "Dynamic control of wavelength switching and shuttering operations in a broadband tunable DS-DBR laser module," in *Proc. Opt. Fiber Commun. Conf. Expo./Nat. Fiber Optic Eng. Conf.*, 2005, Paper OTuE3.

[22] B. Puttnam et al., "Burst mode operation of a DS-DBR widely tunable laser for wavelength agile system applications," in *Proc. Opt. Fiber Commun. Conf./Expo. Nat. Fiber Optic Eng. Conf.*, 2006, Paper OWI86.

[23] T. Segawa, S. Matsuo, T. Kakitsuka, T. Sato, Y. Kondo, and R. Takahashi, "Semiconductor double-ring-resonator-coupled tunable laser for wavelength routing," *IEEE J. Quantum Electron.*, vol. 45, no. 7, pp. 892–899, Jul. 2009.

[24] T. Kanai, N. Nunoya, T. Yamanaka, R. Iga, M. Shimokozono, and H. Ishii, "High-accuracy, sub-μs wavelength switching with thermal drift suppression in tunable distributed amplification (TDA-) DFB laser array," in *Proc. Opt. Fiber Commun. Conf. Nat. Fiber Optic Eng. Conf.*, 2013, pp. 1–3.

[25] T. Gerard et al., "AI-optimised tuneable sources for bandwidth-scalable, sub-nanosecond wavelength switching," *Opt. Exp.*, vol. 29, no. 7, pp. 11221–11242, 2021.

[26] M. C. Larson et al., "Narrow linewidth high power thermally tuned sampled-grating distributed Bragg reflector laser," in *Proc. IEEE Opt. Fiber Commun. Conf./Nat. Fiber Optic Eng. Conf.*, 2013, pp. 1–3.

[27] J. Wesström, G. Sarlet, S. Hammerfeldt, L. Lundqvist, P. Szabo, and P. Rigole, "State-of-the-art performance of widely tunable modulated grating Y-branch lasers," in *Proc. Opt. Fiber Commun. Conf.*, 2004, Paper TuE2.

[28] Y. Ueda et al., "Nanosecond-scale hitless λ-switching of SOA-integrated electro-optically tunable RTF laser with +/-2.5-GHz dynamic frequency accuracy," in *Proc. IEEE Opt. Fiber Commun. Conf.*, 2022, pp. 1–3.

[29] H. L. R. Lira, S. Manipatruni, and M. Lipson, "Broadband hitless silicon electro-optic switch for on-chip optical networks," *Opt. Exp.*, vol. 17, no. 25, pp. 22271–22280, 2009.

[30] Y. Ueda, T. Shindo, S. Kanazawa, N. Fujiwara, and M. Ishikawa, "Electro-optically tunable laser with ultra-low tuning power dissipation and nanosecond-order wavelength switching for coherent networks," *Optica*, vol. 7, no. 8, pp. 1003–1006, 2020.

[31] Y. Ueda, T. Fujisawa, K. Takahata, M. Kohtoku, and H. Ishii, "InP-based compact transversal filter for monolithically integrated light source array," *Opt. Exp.*, vol. 22, no. 7, pp. 7844–7851, 2014.

[32] Y. Ueda, T. Fujisawa, and M. Kohtoku, "Eight-channel reflection-type transversal filter for compact and easy-to-fabricate InC-based optical multiplexer," *J. Lightw. Technol.*, vol. 34, no. 11, pp. 2684–2691, Jun. 2016.

[33] Y. Saito, Y. Ueda, T. Shindo, S. Kanazawa, H. Matsuzaki, and M. Ishikawa, "Burst-tolerant tuning of reflection-type transversal filter laser with single active region," *IEEE Photon. Technol. Lett.*, vol. 34, no. 1, pp. 23–26, Jan. 2022.

[34] J. S. Roberts, J. P. R. David, L. Smith, and P. L. Tihanyi, "The influence of trimethylindium impurities on the performance of InAlGaAs single quantum well lasers," *J. Cryst. Growth*, vol. 195, no. 1–4, pp. 668–675, 1998.

[35] Y. Ueda et al., "Partial regrowth of optical-gain section for improved wafer process flexibility of InP photonic integrated circuits," *J. Lightw. Technol.*, vol. 40, no. 8, pp. 2465–2473, Apr. 2022.

[36] Y. Ueda, Y. Hashizume, T. Yamada, H. Matsuzaki, and M. Ishikawa, "Theoretical and experimental investigation of external-stress effect on quantum-well-based semiconductor interferometer performance," *Appl. Phys. Exp.*, vol. 14, 2021, Art. no. 091005.

[37] ITU-T G.694.1 Telecommunication Standardization Sector Of ITU, "Series G: Transmission Systems And Media, Digital Systems And Networks," *Tranmiss. Media Opt. Syst. Characteristics Opt. Syst.*, Oct. 2020.

[38] G. Agrawal, "Line narrowing in a single-mode injection laser due to external optical feedback," *IEEE J. Quantum Electron.*, vol. 20, no. 5, pp. 468–471, May 1984.

[39] "Integrable tunable laser assembly multi-source agreement," Optical Internetworking Forum, OIF-ITLA-MSA-01.3, Jul. 2015.

[40] T. Baba et al., "Silicon photonics FMCW LiDAR chip with a slow-light grating beam scanner," *IEEE J. Sel. Topics Quantum Electron.*, vol. 28, no. 5, Sep./Oct. 2022, Art. no. 8300208.

Yuta Ueda (Member, IEEE) received the B.E., M.E., and Ph.D. degrees in electrical engineering and bioscience from Waseda University, Japan, in 2007, 2008, and 2011, respectively.

From 2010 to 2011, he was a Research Fellow of the Japan Society for the Promotion of Science. In 2011, he joined NTT Photonics Laboratories, NTT Corporation, Japan. Since 2020, he has been a Visiting Associate Professor with Kyushu University, Fukuoka, Japan. He is currently a Distinguished Researcher with the NTT Device Technology Laboratories. His research interests include semiconductor photonic integrated circuits including tunable lasers and modulators for optical communications and remote sensing systems. He is a Member of the Japan Society of Applied Physics (JSAP) and the Institute of Electronics, Information, and Communication Engineers (IEICE) of Japan.

Yusuke Saito received the B.S. degrees in applied physics from the Tokyo University of Science, Tokyo, Japan, in 2016, and the M.E. degree in electrical and electronic engineering from the Tokyo Institute of Technology, Tokyo, in 2018. In 2018, he joined NTT Device Innovation Center, Japan. His research interests include InP-based photonic integrated devices. He is a Member of the Institute of Electronics, Information, and Communication Engineers of Japan.

Takahiko Shindo (Member, IEEE) received the B.E., M.E., and Ph.D. degrees in electrical and electronic engineering from the Tokyo Institute of Technology, Tokyo, Japan, in 2008, 2010, and 2012. After receiving his Ph.D. degree, he worked as a Research Fellow with the Japan Society for the Promotion of Science. In April 2013, he joined NTT Photonics Laboratories (now NTT Device Innovation Center), NTT Corporation, Japan, where he is currently engaged in research on optical semiconductor devices. Dr. Shindo is a Member of the IEEE Photonics Society, Japan Society of Applied Physics (JSAP), and Institute of Electronics, Information and Communication Engineers (IEICE). From 2010 to 2012, he was the recipient of research fellowship for young scientists from the Japan Society for the Promotion of Science.

Shigeru Kanazawa (Senior Member, IEEE) received the B.E., M.E., and Ph.D. degrees in electronic engineering from the Tokyo Institute of Technology, Tokyo, Japan, in 2005, 2007, and 2016, respectively. In April 2007, he joined Nippon Telegraph and Telephone (NTT) Photonics Laboratories (now NTT Device Innovation Center), Japan. He is engaged in the research and development of optical semiconductor devices and integrated devices for optical communications systems. Dr. Kanazawa is a Senior Member of Photonics Society and Institute of Electronics, Information and Communication Engineers of Japan, and a Member of the Japan Society of Applied Physics and Japan Institute of Electronics Packaging.

Hideaki Matsuzaki (Senior Member, IEEE) received the B.S. and M.S. degrees in physics from Kyoto University, Kyoto, Japan, and the Ph.D. degree in engineering from Toyama University, Toyama, Japan, in 1993, 1995, and 2019, respectively. In 1995, he joined Nippon Telegraph and Telephone Corporation (NTT)'s Atsugi Electrical Communications Laboratories, Japan. He is currently a Senior Research Engineer, Supervisor with NTT Device Technology Laboratories Japan, and engages R&D of compound semiconductor devices, such as InP-HEMTs, HBTs, photo-diodes, and laser-diodes. He is a Senior Member of the Electron Device Society, and Institute of Electronics, Information, and Communication Engineers of Japan, and a Member of the Institute of Electrical Engineers of Japan.

Wataru Kobayashi received the B.S. and M.E. degrees in applied physics and the Dr. Eng. degree in nanoscience and nanoengineering from Waseda University, Tokyo, Japan, in 2003, 2005, and 2011, respectively. In 2005, he joined NTT Photonics Laboratories. He is currently with NTT Device Innovation Center, Japan. His research focuses on the development of optical semiconductor devices. He is a Member of the Institute of Electronics, Information, and Communication Engineers.

Mitsuteru Ishikawa (Member, IEEE) received the B.E. and M.E. degrees in applied physics from the University of Tokyo, Tokyo, Japan, in 1995 and 1997, respectively. In 1997, he joined NTT Opto-Electronics Laboratories, Japan. Since then, he has been involved in development and research on semiconductor-based optical devices for WDM optical communication systems. He is a Member of the Japan Society of Applied Physics and the Institute of Electronics, Information, and Communication Engineers of Japan.